A Grid Connected HRES using Seven Level Inverter - A Hybrid MFO-RBFNN Technique

Mr. Anem Apparo[1*], Dr. G. Chandra Sekhar[2]

[1]*Associate Professor, Department of EEE, Sri Vennkateswara College of Engineering and Technology, Etcherla, Srikakulam, Andhra Pradesh, India*

[2]*Professor, Dept of EEE, GMRIT, Rajam, Srikakulam, Andhra Pradesh, India*

***Abstract* —** *This manuscript proposes an innovative seven-level inverter scheme for grid-connected hybrid renewable energy system (HRES) that comprises wind and photovoltaic (PV) generation subsystems. The proposed controller denotes joint implementation of Moth Flame Optimization (MFO) as well as Radial Base Function Neural Network (RBFNN) and hence it is named as MFO-RBFNN. The purpose of proposed controller is to meet the load power demand and preserve the power regulation (or) maximal energy conversion of wind as well as photovoltaic subsystems. At proposed controller, RBFNN learning process is improved by using MFO algorithm in perspective of minimal error objective function. Here, MFO is utilized to evaluate the optimal gain parameter in view of the variety of source currents from the normal value. It can be useful for building up the optimal control signals dataset. In light of fulfilled dataset, RBFNN performs and forecasts most optimal control signals of seven-level inverter. MFO-RBFNN technique is actualized on MATLAB/Simulink as well as outcomes are examine by two test cases and compared by several solution methods such as base controller, 5 level inverter scheme and MFO-7 level inverter scheme. The comparison results demonstrate that superiority of MFO-RBFNN method and confirm their potential to solve the issue.*

***Keywords* —** *Seven level inverter, grid connected hybrid renewable energy system, converter switching states, wind and photovoltaic generation subsystems.*

I. INTRODUCTION

On a worldwide basis the rapid consumption of fossil fuel resources has needed an alternative energy source to cater current power demand [1]. Developing proof of global warming denotes other key inspiration to decrease our dependence on fossil fuels [2]. Therefore, discovering alternative energy sources is essential to meet the continuously increasing energy demand [3]. The advancement of RES is becoming more popular as well as profitable because there is a negative effect on fossil fuel resources. A wind energy system as well as solar photovoltaic systems denotes generally used RES. As the last decades, this type of RES has been researched [4]. Owing to the lack of electricity grids on remote areas of developing countries, electricity is not accessible today for nowadays over 1,200 million people [5, 6].

The grid-connected power system is financially effectual to extend the power line to the electricity grid [7]. Sometimes when comparing the grid connected hybrid systems with the unique energy source; the grid connected hybrid system is cost effectual to unique source [8]. The most generally utilized energy source is photovoltaic, followed by battery storage [9]. In winter time solar irradiation is lower to late spring, so the hybrid photovoltaic-diesel battery system is more cost-effective. High wind speed areas typically utilize a combination of system for example, hybrid Photovoltaic-Wind-Battery or Photovoltaic-Wind-Diesel-Battery [10-12]. The key drawbacks of such systems are high establishment cost and lower conversion efficiency, yet advancement in these areas of power electronic converters evacuates these conversion efficiency issues [13]. One of the precedents is Maximal Power Point Tracking (MPPT) method utilized at few applications, such as buck, boost as well as bidirectional converter [14].

There are few sorts of MPPT strategies to wind and solar photovoltaic applications [15, 16]. In these systems, MPPT modifies the system quantity to amplify the turbine power output. MPPT algorithms are executed more often than not both DC-DC and AC-DC converters on systems associated with the Photovoltaic-Wind grid in like manner to store excess energy battery banks [17]. Traditional and advanced methods are the classification of MPPT methods. In view of mathematical relationship the traditional technique needs a previous knowledge of system feature that does not satisfy entire meteorological conditions [18, 19]. Subsequently, in any meteorological conditions they can't track correctly the photovoltaic generator or Wind generator MPP [20]. Intelligent MPPT techniques, for example, fuzzy logic (FL) as well as artificial neural network (ANN) is well-organized, however, it is more composite compared with traditional

methods, which is usually easy, cheap as well as less effective [21, 22].

This manuscript an innovative seven level inverter scheme for grid connected hybrid renewable energy system (HRES) that comprises of wind as well as photovoltaic generation subsystems is proposed. The proposed controller denotes joint implementation of Moth Flame Optimization (MFO) as well as Radial Basis Function Neural Network (RBFNN) and hence it is named as MFO-RBFNN. The purpose of proposed controller is to meet the load power demand as well as preserve the power regulation (or) maximal energy conversion of wind as well as photovoltaic subsystems. Remaining manuscript is classified as take after; current investigation work and research work background are mentioned in Section 2. Mathematical modelling of hybrid renewable energy system as well as proposed seven-level inverter topology is explained on Section 3. Optimal control scheme of grid connected HRES using proposed controller uses is depicted in Section 4. The suggested method accomplishment outcomes and related consultation are provided at Section 5 and manuscript is concluded on Section 6.

II. RECENT RESEARCH WORKS: A BRIEF REVIEW

Recently there have been several research works at bibliography that depends on optimal control of grid-associated hybrid renewable energy sources, for instance, wind-photovoltaic (PV) system using various techniques as well as various perspectives. Few of them are reviewed as here.

With the switch count decreased, 3-ϕ, multilevel inverter (MLI) optimized topology setup for five or greater level operation was displayed by A. Hota et al. [23] Two basic units (BU) of multi-level converter and one 3-level inverter structured in T (3-LI) are introduced in system. Among the three phases that maintain symmetry, accordingly BUs is shared equally. To create as pulse switch to BUs as well as 3-LI, an algorithm was additionally conceived utilizing a carrier-based space vector modulation method. For the transformer less PV system 3-ϕ cascaded inverter by leakage current decrease was explored by X. Guoin *et al.* [24]. The common mode loop model of the H4 three-phase cascade inverter connected to conventional grid was introduced. Leakage current, common mode voltage as well as differential mode voltage ratio was further analyzed. A new three-phase cascade H5 grid connected inverter as well as their modulation technique is used to solve the issue.

E. Grover-Silva et al. [25] have shown an Optimal Power Flow (OPF) distribution grid planning tool to integrate battery sizing, placement as well as operation methods. An alternating current (AC) multi-temporal OPF algorithm was introduced; the algorithm utilizes a convex relaxation of power flow equations by large algorithmic performance. An algorithm was one of a kind and creative because of the way, which consolidates the instantaneous optimization of placement as well as storage device size. To diminish the recovery time of photovoltaic system, A. Guichi et al. [26] have outlined a PV Customer Grid Supply System (PCGSS) by bi-directional power flow. At that point, excess energy was conveyed to the grid; similarly, grid supplies the loads directly. Based on this reason, another management algorithm was used for optimizing a power generated. Inside the utility grid, it allows the system to act from distributed source. With the help of demand side management, a multi-objective optimization technique together optimize the planning as well as operation of grid-tied microgrid to different distributed generation sources like wind turbine as well as PV array was introduced by J. Chen et al. [27] Fuzzy satisfaction maximization technique was received to take care of multi-objective optimization issue.

A. Background of the Research Work

A review of current investigation operation demonstrates that effectual control of grid-connected hybrid generation scheme using solar as well as wind power denotes important contributing component. Be that as it may, variations in load demand, meteorological data, for instance, irradiation, temperature as well as wind speed are dominant problems at hybrid PV-wind applications associated with the grid. These disturbances occur mainly due to the complicated control of variety of energy sources. Many procedures have been implemented to control hybrid renewable energy generation, for example Active Power Control by anti-windup PI controller, Fuzzy Logic Control, Genetic Algorithm as well as Particle Swarm Optimization, etc. APC and AWPI have been implemented to high level of performance by decreased number of sensors to stable operation of wind-photovoltaic-battery hybrid grid-depend on power generation system; though it is not appropriate to complex micro grid and also does not consider total cost of generation. Fuzzy logic control consists of capability for removing maximal power point of photovoltaic generator (PVG) as well as wind generator. Be that as it can, it needs a lot of data. Not useful for programs a great deal of lower or higher to historical data. GA and PSO consist of capability to approximate the cost of energy (COE). The main drawbacks of these algorithms are very slow implementation and they cannot find as correct solution either. Although the previous strategies are used to control and dissect disturbances from renewable energy sources, the complexity of algorithm is large due to greater amount of testing needed. To defeat this difficulty, optimal control utilizing advanced technology is necessary. In related works, some control methods are shown to

optimal control the hybrid power generation associated with grid; the restrictions mentioned above have been generated to carry out this investigation work.

III. GRID CONNECTED HRES USING SEVEN LEVEL INVERTER TOPOLOGY

In this section, the grid connected HRES using seven level inverter is explained. The block diagram of grid associated HRES using Seven Level inverter by aid of proposed controller is portrayed at Fig 1. The block diagram has grid-associated hybrid renewable energy sources (HRES), for instance, PV and wind, seven-level inverter, PI controller, and pulse width modulation situated towards the end of load. The solar photovoltaic system includes a photovoltaic matrix as well as DC-DC converter. The wind energy system consists of wind turbine by permanent magnet synchronous generator (PMSG), DC-DC converter, as well as AC-DC three-phase uncontrolled rectifier. At point when the parameters of the sources are given to the input of Seven Level inverter, the output signal is flow through the load. The purpose of proposed controller is fulfilling the load power demand and keeps up power regulation of the wind and PV subsystems. Based on this control scheme, system parameter variant as well as external disturbances are decreased and load demands are optimally fulfilled. Brief descriptions of blocks are explained on accompanying sub sections. Initially, mathematical demonstration of HRES system is portrayed as follows,

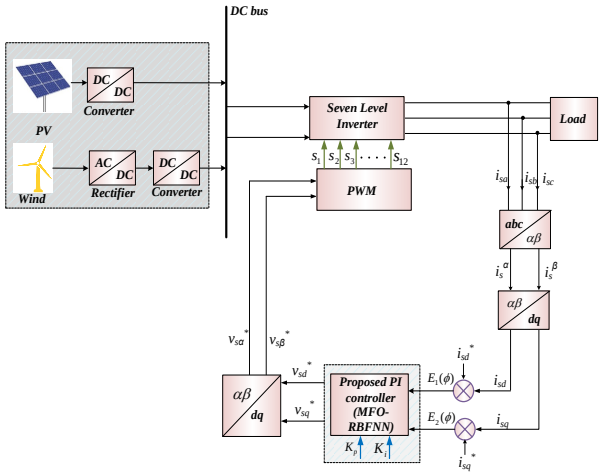

Fig 1. Block diagram of grid associated HRES using Seven Level Inverter with proposed controller

A. *Mathematical Modelling of Hybrid Renewable Energy Sources (HRES)*

These sections, numerical determination for both wind and PV system is formulated as below,

1) ***PV System Modeling:*** Dynamic model of photovoltaic system is clarified in this subsection and the relationship among output current of individual photovoltaic cell as well as output voltage can be acquired depending on the attached equation [28],

$$v_{pv} = \frac{1}{c}\left[i_{pv} - i_{dc}\zeta_{pv}\right] \tag{1}$$

here v_{pv} represent voltage level at the terminals of photovoltaic panel, i_{pv} denotes current generated to PV array, C electrical parameter of converter, i_{dc} current injected on dc bus, ζ_{pv} control signal of dc-dc converter. The equation for the current generated to PV array is derived as below,

$$i_{pv} = x_p i_p - x_P i_{rev}\left(e^{\frac{q\left(v_{pv}+i_{pv}r_s\right)}{x_{se}\Delta_c KT}} - 1\right) \tag{2}$$

here x_P is the number of series strings at parallel, i_p denotes photocurrent, i_{rev} is the reverse saturation current, x_{se} indicates count of photovoltaic cells connected at series, Δ_c denotes cell deviation, K indicates Boltzman constant as well as T denotes cell temperature.

2) ***Wind Power System Modeling :*** The wind turbine power equation is derived using the following equation,

$$p_{wt} = \begin{cases} p_{rated}\dfrac{v_k - V_k^c}{V_k^{rated} - V_k^c} & v_c \le v \le v_{rated} \\ p_{rated} & v_{rated} \le v \le v_{cf} \\ 0 & v < v_c \text{ and } v > v \end{cases} \tag{3}$$

here, p_{rated} indicates electrical power rated, v_c denotes wind speed cut-in, v_{rated} indicates wind speed rated, v_{cf} denotes wind speed cut-off, k indicates Weibull shape parameter that depend on wind speed distribution.

B. *Constraints of the System*

There are two restrictions that are assumed for grid connected HRES control scheme. They are power balance restrictions for every system as well as creating capacitance constraints. The equation of this restriction is represented as below,

1) ***Power Balance Constraints: At*** power balance constraints, aggregate power generation of photovoltaic as well as wind system should be similar from load. The equation for this condition is,

$$p_{pv} + p_{wt} = p_{load} \quad (4)$$

here p_{pv} denotes photovoltaic output power, p_{wt} denotes output power of wind, and p_{load} denotes total power generation of load.

2) ***Generation Capacity Constraints of the System:*** System generation capacity limitations must be limited among maximal and minimal values with the end goal to balance out the system performance.

$$p_{\min}^{j} \le p^{j} \le p_{\max}^{j} \quad (5)$$

where $p_{\min}^{j}$ and $p_{\max}^{j}$ is the minimal as well as maximal value of power generation of renewable energy resources at *jth* unit.

C. Proposed Seven-Level Inverter Topology

These sections, a seven level inverter topology is described. In this manuscript, a seven-level inverter topology is developed to provide a large number of output levels using a small number of components. The proposed seven-level inverter topology is shown at Fig. 2. From additional clamping diodes or voltage balance capacitance, this inverter can keep up a strategic distance. The technique to calculate the approximations of needed DC voltage sources is also established. For every inverter level can generate distinctive outputs of voltage. At that point the Seven-Level Inverter output voltage is given by,

$$v_0 = v_1 + v_2 + v_3 + \cdots v_m \quad (6)$$

here m is denoted as the number of stages in cascaded i.e. $m = 7$. To produce as count of levels, output phase voltage level and number of diode is resolved utilizing different approaches. From that point forward, the new switching devices arrangement is calculated. A Seven-Level Inverter topology contains various H-Bridge inverter units related at series and supported as discrete DC sources. DC sources must be isolated one another as output is taken at series. Keeping in mind, terminate goal to achieve greater voltage levels, Seven-Level Inverter is proposed to be utilized with PV and wind sources. Every H-Bridge consists of property to make three voltage levels like $+v_{dc}$, 0, $-v_{dc}$ where v_{dc} is input voltage of H-Bridge. To cascade three H-bridge inverter circuits by each H-bridge encourages as various DC source, Seven-Level Inverter is obtained. Output level quantity a at each stage is recognized by number of H-bridge inverter unit's "n" with Equation (7).

$$a = b + 1 \quad (7)$$

For $b = 2n$, number of inverter level as a, number of full bridge connected at series is represented as n. To obtain seven-level output, the previous switching pattern is used [29]. Seven-level inverter output voltage waveform with $\delta_1, \delta_2, \delta_3$ talking at switching angles is used to harmonic reduction. By phase shift, the switching time of positive as well as negative phase legs of inverter, each complete bridge creates a quasi square waveform. Here, level number (a) are seven, therefore the number of series associated full bridge inverter circuits are three that called as Equation (6). Switching devices of proposed inverter should be selected precisely, on basis, which voltages of each device are distinctive. The voltage of switches $s_1 \ldots s_{(n-1)}$ amid their OFF state is $v_{dcs1} \ldots v_{dcs(n-1)}$, which is used to fulfil the following condition (8) as

$$v_{dcs1} \ldots v_{dcs(n-1)} = \frac{2}{2n+1} \sum_{d=0}^{n} v_d \quad (8)$$

The switching frequency of this switch is twice the frequency of reference waveform. Based on this method, MOSFET as well as insulated gate bipolar transistor (IGBT) is appropriate to this switch. In this work, MOSFET switch is used for the reason; the voltage of the switches winds up noticeably litter and contrasts by output voltage while number of levels is increased.

1) Losses Calculation: *The* power electronic equipment, for example, inverter contains switching devices and the operation of inverter produces harmonics in the current and voltage into the system from which they are working [30]. Through the injection of harmonics these harmonics influence the equipments operation associated with a similar system. Also in the operation of working mode predominantly in the losses of switching, the conduction losses and switching losses are considered principally. These losses can be executed by various systems. The clarifications of the losses are definite as takes after.

(a) Analysis of Conduction Losses: When the power device is ON state and conducts current, conduction loss can occur. Accordingly, by increasing the voltage drop in ON state during conduction, the power dissipation is processed through current flows via device, which is derived as follows (9),

$$s(t) = v_{ON}(t) \times i(t) \quad (9)$$

where the ON states saturation voltage as $v_{ON}(t)$ and the power device current as $i(t)$. The bidirectional switch of saturation voltage is analyzed,

which is the whole of diode saturation voltage which is estimated to linear function, MOSFET, acquired from the makers.

$$v_{ON}(t) = v_{ON}^{\ MOSFET} + v_{ON}^{\ diode} \tag{10}$$

Here

$v_{ON}^{\ MOSFET} = v_T + r_T \times i^{\gamma}$,

$v_{ON}^{\ Diode} = v_{diode} + r_{diode} \times i$.

where threshold voltages of power devices indicated as v_T and v_{diode} , equivalent resistances of voltage drop over the power devices as r_T *and* r_{diode} and constant is γ . The inverter creates a large number of levels; output current may be considered sinusoidal. Along these lines, in the bidirectional switch the instantaneous conduction losses can be composed as follows,

$$s(t) = v_T \times i_p \sin(\omega t) + v_{diode} \times i_p \sin(\omega t) + r_{diode} \times i^2{}_p \sin^2(\omega t) + r_T \times i^{\gamma+1}{}_p \sin^{\delta+1}(\omega t) \tag{11}$$

where the peak value of output current signified as i_p . Clearly, a switch turns ON at various operation modes of a seven level inverter, by exception of the zero voltage level.

(b) Analysis of Switching Losses: Switching losses are power dissipation due to turn ON and OFF switching transitions and this loss are due to faulty switching of devices. Incorporation of the ON voltage result as well as current waveforms of switching period can acquire the switching losses. The energy losses may be obtained through incorporating the result of voltage as well as current waveforms in switching period from below,

$$\varepsilon_{OFF} = \frac{1}{n}\left(i^2 r T_{OFF} \Big/ 6 \right) \tag{12}$$

here the snubber resistor as r and the fall time of device as T_{OFF} and RMS estimation of output current as i . Energy loss is figured at switch operation, turn-ON period is composed from takes after,

$$\varepsilon_{ON} = \left(v_{dc} + \Delta v_c + v_D\right) \times \left(I + \frac{n\left(v_{dc} + \Delta v_c\right)}{r} \right) \times \frac{T_{ON}}{6} \tag{13}$$

where voltage drop across the snubber resistor, $v_D = ri/n$, the rise time of the MOSFET device as T_{ON} and $\Delta v_c = \frac{i\kappa}{nc}$. The delay time to provide the safe commutation of switches is represented as κ .

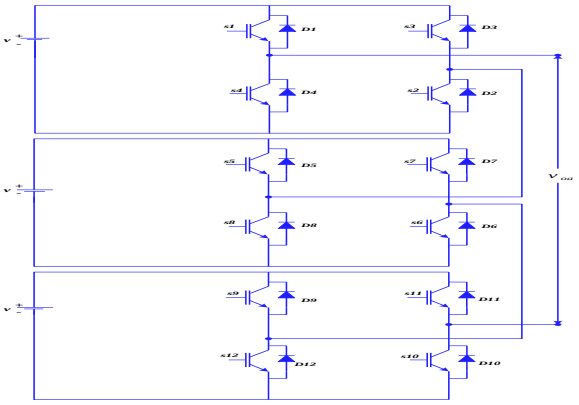

Fig . 2. Proposed Seven-Level Inverter topology

D. Control Analysis and Working Structure of Proposed Controller

In this sub section, the control analysis and working structure of proposed controller is studied. At first, the 3ϕ supply is given as the input to the inverter and the proposed inverter is associated with the load. Here, the 3ϕ source voltage and currents are analyzed. At first, the 3ϕ quantity of current signals is given to the Clarke's transformation. In this change, the current signals (i_{sa}, i_{sb}, i_{sc}) are at first changed to the orthogonal stationary frame at $\alpha\beta$ using Clarke's transform and after that synchronous rotating reference frame (d-q) to utilize Park's transformation. Outflow of abc- $\alpha\beta$ transformation, the 3ϕ quantities is changed over into 2ϕ quadrature quantities using Clarke's transform are depicted in the following equation (14).

$$\begin{bmatrix} i_s^{\alpha} \\ i_s^{\beta} \end{bmatrix} = \sqrt{2/3} \begin{bmatrix} 1 & -1/2 & -1/2 \\ 0 & \sqrt{3}/2 & -\sqrt{3}/2 \end{bmatrix} \times \begin{bmatrix} i_{sa} \\ i_{sb} \\ i_{sc} \end{bmatrix} \tag{14}$$

The transformation from $\alpha\beta$ to d-q reference frame using Park's Transform is portrayed in equation,

$$\begin{bmatrix} i_{sd} \\ i_{sq} \end{bmatrix} = \begin{bmatrix} \sin\omega t & -\cos\omega t \\ \cos\omega t & \sin\omega t \end{bmatrix} \times \begin{bmatrix} i_s^{\alpha} \\ i_s^{\beta} \end{bmatrix} \tag{15}$$

From that transformation, the output signal of i_{sd}, i_{sq} is compared to the reference dq current source i_{sd}^*, i_{sq}^* by using the comparator to produce the error signal. The output error signal is formulated as follows,

$$e = e_1 + e_2 \tag{16}$$

Where

$$e_1 = i^*_{sd} - i_{sd} \tag{17}$$

$$e_2 = i^*_{sq} - i_{sq} \tag{18}$$

here the PI controller enhancement is depend on the two parameters value they are K_P and K_I. Thus, there is a requirement to tune these two parameters based on the specific application. During the time of process, the error signal is calculated under the proposed control function. At the same time, the output signal is given to the proposed controller. In the proposed controller operation, the MFO technique is performed. From the output of proposed controller, it is shaped as a dataset and furthermore put away as the corresponding gain parameter values. At that point the optimal best value is assessed utilizing the RBFNN. The output of RBFNN is connected to the PI controller and to create the optimal control pulses. Keeping in mind the end objective to generate reference voltage signals (v^*_{sd}, v^*_{sq}) and to change them back to original frame, inverse transformation ought to be done from d-q to α-β frame. Inverse park's transformation as d-q to α-β reference frame is communicated in following condition (19),

$$\begin{bmatrix} v_s^\alpha \\ v_s^\beta \end{bmatrix} = \begin{bmatrix} \sin\omega t & \cos\omega t \\ -\cos\omega t & \sin\omega t \end{bmatrix} \times \begin{bmatrix} v^*_{sd} \\ v^*_{sq} \end{bmatrix} \tag{19}$$

Finally, the optimized output voltage signal is performed to control the switching operation of inverter.

1) PI controller: Proportional integral (PI) controllers are utilized to control the proposed inverter for less demanding execution. There have been significant research works done in the control area utilizing PI control method to reduce Total Harmonic Distortion (THD) and build up a new proposed inverter. In this work, the PI controller forms the error signal and creates the required reference voltage to drive the error to zero. The procedure of PI controller is represented in figure 4. Here, the error signal of $e(s)$ is assessed from equation (12) is utilized to decide the control signal for PWM modulator to assess the gating pulses for power switches. The controller input is an error signal of current signals acquired from the reference current and inverter current. The PI controller output is spoken to as voltage signals. The assurance of control signal for PWM modulator by the proposed MFO-RBFNN controller is updated based on the accompanying equation,

$$v(s) = K_P e + K_I \int_0^s e\,dt \tag{20}$$

In view of the above condition, the output voltage is dictated by precise tuning of the gain parameters for accomplishing the optimal outcomes. With respect to, to assess the optimal parameters the MFO-RBFNN controller is used. From that point onward, the optimal gain parameter is accomplished while optimizing the gain parameters and limiting the error signals. The optimized signals are controlled by utilizing the accompanying equation,

$$v^s_{op} = K_P e + K_I \int_0^s e\,dt \tag{21}$$

where v^s_{op} speaks to the control signal determined by MFO-RBFNN controller. Execution of a PI controller is subject to the estimation of two parameters, for example K_P, K_I. These gains are enhanced by the MFO-RBFNN.

IV. OPTIMAL CONTROL SCHEME OF GRID CONNECTED HRES USING PROPOSED CONTROLLER

In this section, the detailed process of MFO-RBFNN technique is analyzed for the seven-level inverter. The proposed controller is the combined execution of Moth Flame Optimization Algorithm (MFO) as well as Radial Basis Function Neural Network (RBFNN) and hence it is named as MFO-RBFNN. The aim of the proposed control technique is for satisfying the load power requirement as well as for maintaining the regulation of power (or) maximal energy conversion of the wind as well as solar subsystems. At first, MFO is performed for controlling the error function and formed a dataset. After that, the best optimal control pulse is determined using the RBFNN. The detailed process of the proposed controller is described as below,

A. MFO Based Dataset. Generation

The moth-flame optimization is a meta-heuristic nature-roused optimization algorithm, which is called transverse orientation of the course procedure for moths in nature [31]. In this paper, MFO is utilized to enhancing the efficiency of PI controller. From control purpose, the input as well as gain parameter is initialized for determining the objective function. The main objective function of this dissertation is minimization of error signal. Here, the input of reference dq current source is analyzed. The minimized objective function can be evaluated from the inputs. The optimal output is defined in terms of assessed inputs. In this regard the following

equations have been developed. The process of the proposed controller is briefly explained given below:

Layer 1: Initialization

Initialize the moths input population such as error signals of currents. The set of *m* moths are equated as a matrix which is done based on the following equation,

$$X = \begin{bmatrix} x_{1,1} & x_{1,2} \cdots & x_{1,p} \\ x_{2,1} & x_{2,2} \cdots & x_{2,p} \\ \vdots & \vdots \cdots & \vdots \\ x_{m,1} & x_{m,2} \cdots & x_{m,p} \end{bmatrix} \quad (22)$$

here m as the moth's number, p as number of parameters.

Layer 2: Random Generation

After the process of initialization, random generating the gain parameters of PI controller and the corresponding equation is formulated as follows,

$$RD^i = \begin{bmatrix} K_P^{11}K_I^{11} & K_P^{12}K_I^{12} & \dots & K_P^{1n}K_I^{1n} \\ K_P^{21}K_I^{21} & K_P^{22}K_I^{22} & \dots & K_P^{2n}K_I^{2n} \\ \vdots & \vdots & \vdots & \vdots \\ K_P^{m1}K_I^{m1} & K_P^{m2}K_I^{m2} & \dots & K_P^{mn}K_I^{mn} \end{bmatrix} \quad (23)$$

here RD^i is represented as random generation.

Layer 3: Evaluation

The fitness function of moths is assessed as their objective function of the proposed controller. The function $F(s)$ is given by,

$$F(s) = Min\{e\} \quad (24)$$

Where, $Min\{e\}$ represents the minimization of error function.

Layer 4: Updation

Using the following equation the moth position is updating as for the flame in light of the fitness function

$$Y_{ij}^s = Z_{ij}\, e^{brd} \cos(2\pi r) + f_j, \quad j = 1,2,\dots,m \quad (25)$$

$$Z_{ij} = \left| f_j - Y_{ij} \right| \quad (26)$$

where the moth with the spiral function indicated as Y_{ij}^s, the distance between the i^{th} moth and j^{th} flame is signified as Z_{ij}, the j^{th} flame of MFO algorithm as f_j, spiral shape constant to characterize the logarithmic spiral shape as b as well as random number uniformly distributed in [-1, 1] is represented as rd.

Layer 5: Termination

At termination stage the better solution is selected in terms of the fitness function. The optimization process better value is indicated as e^{best} and $K_P^{best}K_I^{best}$. The best dataset of the optimization parameters are defined as follows,

$$\begin{bmatrix} e^{11} & e^{12} & \dots & e^{1n} \\ e^{21} & e^{22} & \dots & e^{2n} \\ \vdots & \vdots & \vdots & \vdots \\ e^{m1} & e^{m2} & \dots & e^{mn} \end{bmatrix} = \begin{bmatrix} K_P^{11}K_I^{11} & K_P^{12}K_I^{12} & \dots & K_P^{1n}K_I^{1n} \\ K_P^{21}K_I^{21} & K_P^{22}K_I^{22} & \dots & K_P^{2n}K_I^{2n} \\ \vdots & \vdots & \vdots & \vdots \\ K_P^{m1}K_I^{m1} & K_P^{m2}K_I^{m2} & \dots & K_P^{mn}K_I^{mn} \end{bmatrix} \quad (27)$$

Therefore, best combination of error signals and the PI controller gain parameters can be demonstrated.

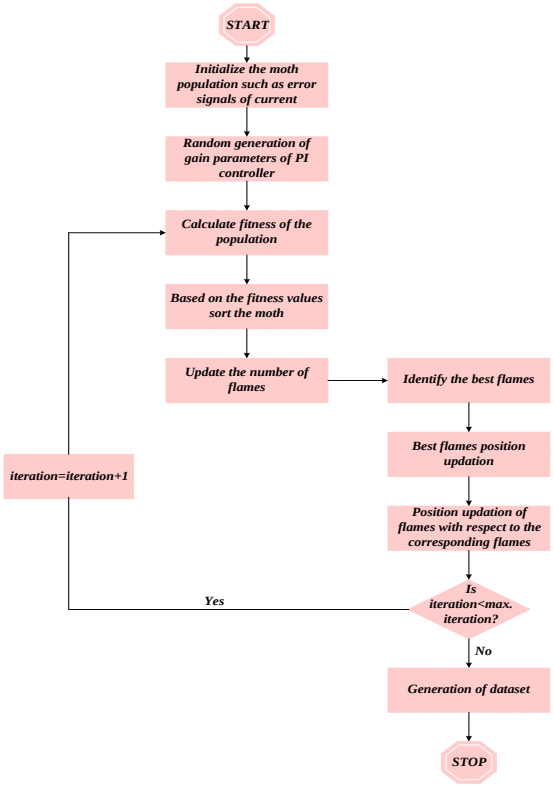

Fig. 3. Flowchart of dataset generation using MFO technique

Layer 6: Save the optimal results

The optimal results are received by utilizing the objective function when the above process is completed. Until the maximum iteration is reached the above procedure is repeated. Based on that, optimal outputs are formed as a dataset and trained for RBFNN. The flowchart of dataset generation using MFO technique is depicted in Fig 3. The working procedure of RBFNN is described in the following,

B. RBFNN Based Optimal Control Signals Determination

By utilizing the RBFNN system, prediction of optimal control parameter is performed. RBFNN is considered a feed-forward network consisting of three layers of neurons [32]. Input layer is the first layer as well as it contains the source nodes for input data. Single hidden layer in the network is the second layer, which is composed of radial basis functions. Non-linear transformation is used through these functions from input layer to hidden layer. The output layer is the third layer and is structured by linear combination of function response. Detailed steps of RBFNN system are made cleared in the following section,

***Step* 1:** The input vector G is used at the input layer of the network. Input vector G is given by the following equation,

$$G = \left[G_1 \; G_2 \cdots G_p \right]^T \tag{28}$$

here *G* indicates input vector of RBFNN.

***Step* 2:** Gaussian function in hidden layer is assumed as radial basis function that is defined as given below,

$$H_j(x) = \exp\left(-\frac{\left\| G - \vartheta_j \right\|^2}{\lambda_j^2} \right) \quad where\ j = 1,2,\cdots,m \tag{29}$$

here Euclidean norm can be represented as $\|.\|$, the j^{th} neuron of the hidden layer as *j*, count of hidden neurons as *m*, centres, width of the Gaussian function is indicated as ϑ_j and λ_j.

***Step* 2:** The output of RBFNN is structured as a linear combination of the outputs of hidden neurons in output layer, which is derived as follows,

$$\begin{aligned} N_i(x) &= \sum_{j=1}^{m} W_{i,j}\, H_j(x) \quad where\ i = 1,2,\cdots,o \ and \ j = 1,2,\cdots,m \\ &= W_i^T H(x) \end{aligned} \tag{30}$$

here hidden output vector is represented as $H = [H_1,\cdots,H_m]^T$; weights vector of the network can be represented as $W_i = [W_{i,1},\cdots,W_{i,j}]^T$, connective weight among j^{th} hidden neuron as well as o^{th} neuron of output layer as $W_{i,j}$.

***Step* 4:** RBFNN learning stage is performed by updating weights as well as biases to reduce the mean-squared-error performance index (MSE) that is defined as,

$$K_T(t) = [C_T^f(t)] \tag{31}$$

where $C_T{}^f(t)$ is represents the output or target signal. Then the proposed MFO-RBFNN technique is minimized the error signal and optimally determines the control signals while optimizing the PI controller gain parameters. The structure of RBFNN is portrayed in Fig 4.

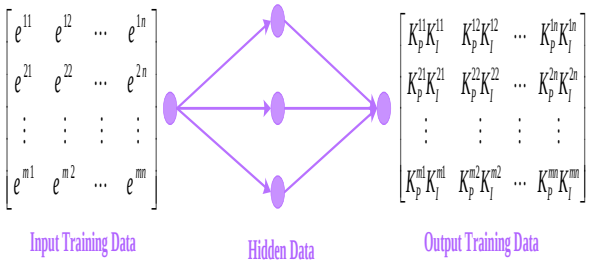

Fig. 4. Structure of RBFNN

V. SIMULATION RESULTS AND DISCUSSIONS

The result of simulation and discussion is studied at this section. In order to evaluate the MFO-RBFNN technique for a grid connected hybrid system includes wind as well as photovoltaic generation subsystems using seven level inverter schemes is presented. The MFO-RBFNN-7 level inverter scheme is implemented at the work site of MATLAB/Simulink as well as performance has been compare with various techniques such as base, 5 level and MFO-7 level. The following section reports the case studies to optimally satisfying the load power requirement as well as for maintaining the regulation of power of the wind and PV subsystems using MFO-RBFNN technique is explained below here. Here, two test cases are considered. They are deviation in load condition and deviation in renewable energy sources. The simulation results of each case is plotted as follows,

Case 1: Deviation in load condition:

At this case, deviation in load condition is simulated and performance of the proposed controller in this condition is also studied. Figure 5 (a) shows graph of irradiance (W/m^2) versus time (sec). At load deviation condition, the irradiance of solar is kept as constant along the value of 1000 W/m^2. The graph of wind speed (m/s) versus time is appeared at Figure 5 (b). This figure shows wind speed is also kept as constant in the load deviation condition with the value of 10 m/s. Figure 6 (a) depicts wind power of proposed controller versus time. This figure shows wind power attains the maximum power of 1600 w at time instant t=0.15 to 1 sec. Fig 6 (b) shows the PV power of proposed controller versus time. The PV power at time instant of 0.12 to 1 sec it reaches maximum power of 5800 w. Fig 6 (c) plots the wind power comparison graph

of proposed controller over the existing approaches. This figure shows base method achieve the maximum power of 1642 w, the 5 level inverter observes the maximum power of 1644 w, the MFO-7 level technique accomplishes the maximum power of 1645 w and the proposed controller accomplishes the maximum power with the optimal value of 1648 w. The PV power comparison plot of proposed controller over the existing technique is appeared in Fig 6 (d). It is observed from the figure, the base method accomplishes the maximum power of 5762 w, the 5-level inverter achieves the maximum power of 5765 w, the MFO-7 level scheme obtains the maximum power of 5768 w and the proposed controller acquires the maximum power optimally with the value of 5771 w.

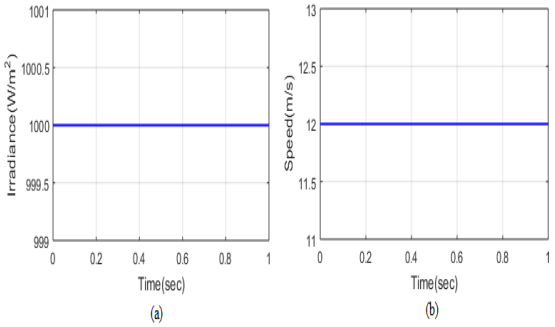

Fig. 5. (a) Irradiance (b) Wind Speed

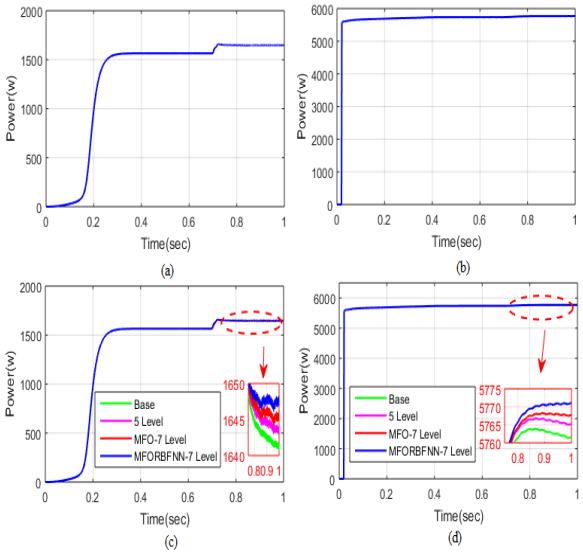

Fig. 6. (a) Wind power of proposed controller (b) PV power of proposed controller (c) Wind power comparison (d) PV power comparison

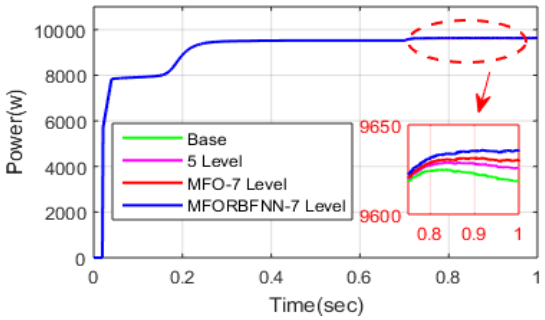

Fig. 7.Total power (Wind and PV) comparison

Fig 7 shows the total power comparison of RESs like wind and photovoltaic of proposed controller along existing techniques. Figure 7 shows base method attains the maximum power of 9620 w; the 5 level inverter scheme reaches the maximum power of 9625 w, the MFO-7 level inverter gets the maximum power of 9630 w and the proposed controller earns the maximum power with the optimal value of 9635 w. Fig 8 depicts the grid power of proposed controller with respect to time. The grid power of proposed controller produces the maximum power of 2300 w. Figure 9 (a) depicts load power of proposed controller versus time.

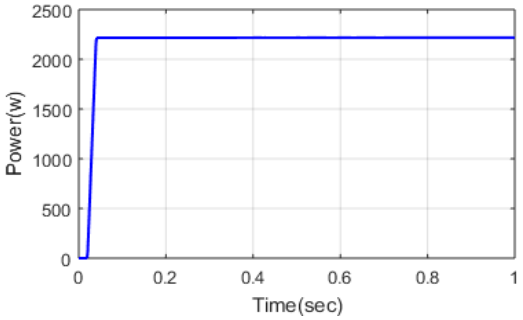

Fig. 8. Grid power of proposed controller

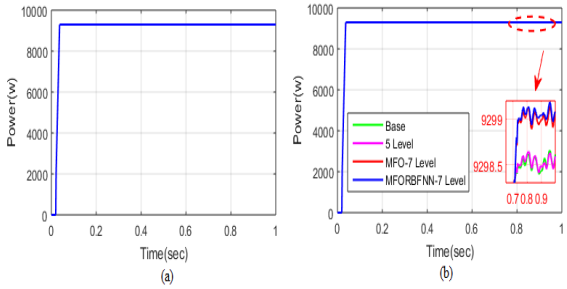

Fig .9. (a) Load power of proposed load power controller (b) Load power comparison

This figure shows load power of proposed controller procures the maximum power of 9100 w. Figure 9 (b) shows proposed controller load comparison graph as well as existing techniques. This figure shows the base method achieves maximum power of 9298.51 w, the 5-level inverter scheme generates the maximum power of 9298.53 w,

the MFO-7 level inverter scheme produces the maximum power of 9299.35 w and the proposed controller achieves the maximum power of 9299.55 w. The plot of seven-level inverter voltage of proposed controller is plotted in Fig 10. As seen from the fig 10, the voltage of the seven-level inverter achieves the voltage range of 150 V at the time instant of t=0.6 to 1 sec.

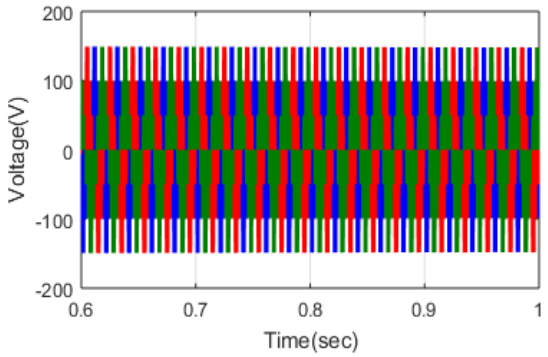

Fig. 10. Seven-level Inverter voltage of proposed controller

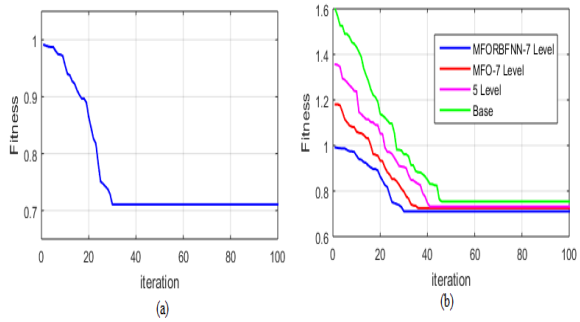

Fig.11. Convergence Analysis (a) proposed controller (b) Comparison of Proposed controller and existing techniques

Figure 11 (a) depicts proposed controller fitness graph with iteration count of 100. As seen from the Fig 11 (a), at the count of iteration of 20, fitness reaches the value of 0.89 and in count of iteration at 30, fitness value is 0.71. The fitness comparison of proposed controller and the existing technique is plotted at figure 11 (b). As seen from the figure 11 (b), base method converge in the count of iteration at 44, 5 level inverter scheme converges at the count of iteration at 42, the MFO-7 level inverter scheme converges at the count of iteration at 36 and the proposed controller converge in the count of iteration at 30. Table 1 tabulates the statistical analysis of proposed controller with various techniques for deviation in load condition. The statistical analysis parameters like mean, median, standard deviation are tabulated. Based on table 1, proposed controller mean value is 0.7633, the proposed controller median value is 0.7107, and proposed controller standard deviation is 0.0954. The proposed method gives best result than the various existing techniques.

TABLE 1
STATISTICAL ANALYSIS OF PROPOSED CONTROLLER WITH DIFFERENT TECHNIQUES FOR DEVIATION IN LOAD CONDITION

Solution Techniques	Mean	Median	Standard Deviation
Base	0.9278	0.7539	0.2567
5 Level	0.8571	0.7318	0.1912
MFO 7 Level	0.8072	0.7253	0.1386
MFORBFNN 7 Level	0.7633	0.7107	0.0954

Case 2: Deviation in Renewable Energy Sources

Deviation in RESs is simulated and the proposed controller performance in this condition is also investigated at this case. Fig 12 (a) depicts the plot of irradiance versus time. The irradiance in this case varies at the time instant of t=0.5 to 0.79 and the value of irradiance decreases from 1000 to 500 W/m^2 and after that at the time instant of t=0.79 to 0.1, the irradiance value goes to normal condition. Fig 12 (b) shows the graph of wind speed versus time. The wind speed in this case goes to constant value with the value of 12 m/s.

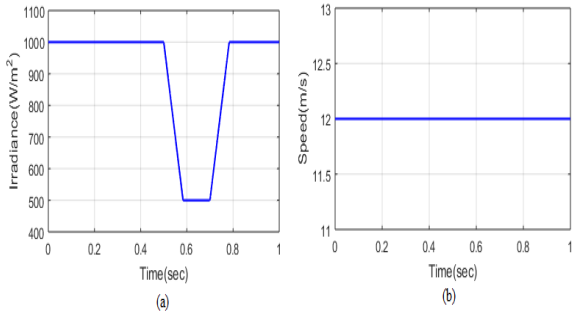

Fig .12. (a) Irradiance (b) Wind Speed

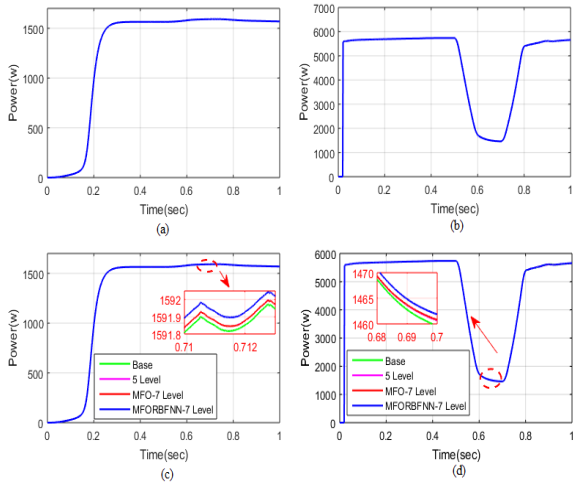

Fig. 13. (a) Wind power of proposed controller (b) PV power of proposed controller (c) Wind power comparison (d) PV power comparison

Fig 13 (a) depicts wind power of proposed controller versus time. Fig 13 (a) shows wind power attains the maximum power of 1600 w at the time instant t=0.15 to 1 sec. PV power of proposed controller versus time is depicted in Fig 13 (b). The PV power at the time instant of 0.12 to 0.5 sec it reaches maximum power of 5700 w. Also at the time instant of t=0.5 to 0.8 sec, power value drops to 1500 w and after that the PV power goes to the initial value of 5700 w. Fig 13 (c) plots the comparison graph for wind power of proposed controller over the existing techniques. Fig 13 (c) shows base method achieve the maximum power of 1591.91 w, the 5 level inverter observes the maximum power of 1591.93 w, the MFO-7 level technique accomplishes the maximum power of 1591.95 w and the proposed controller accomplishes the maximum power with the optimal value of 1592 w. The proposed controller photovoltaic power comparison plot over the existing techniques is appeared at Figure 13 (d). It is observed from the figure, the existing methods are deviated from the optimal value and it doesn't give the maximum power. On the other hand, the deviation of renewable energy sources, the proposed controller gives optimal power than the existing techniques.

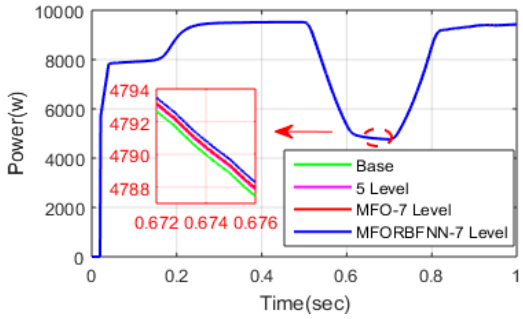

Fig. 14. Total power (Wind and PV) comparison

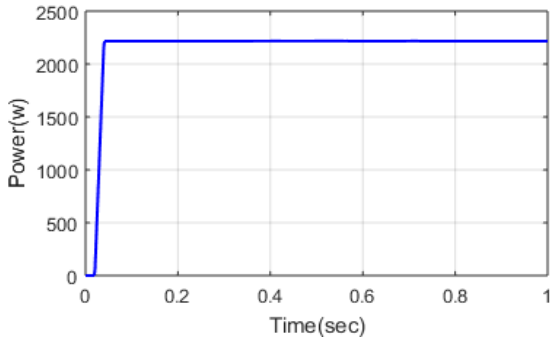

Fig. 15. Grid power of proposed controller

Fig. 14 depicts the total power (PV and wind) of proposed controller over the existing techniques. Figure 14 shows the base method accomplishes maximum power of 4792.1 w, the 5 level inverter scheme achieves the maximum power of 4792.3 w, the MFO-7 level inverter scheme reaches the maximum power of 4792.5 w and the proposed controller attains the maximum power of 4793 w. Figure 15 shows the grid power of proposed controller. Figure 15 shows the grid power at the time instant of t=0.12 to 1 sec it gives maximal amount of power of 2300 w. The load power of proposed controller versus time is delineated in Fig 16 (a). Figure 16 (a) shows the load power of proposed controller procures the maximum power of 9100 w. Fig 16 (b) shows the graph of load power comparison of proposed controller as well as existing techniques. These figures shows the base method achieves the maximum power of 9297 w; the 5-level inverter scheme generates the maximum power of 9297.2 w, the MFO-7 level inverter scheme produces the maximum power of 9297.4 w and the proposed controller achieves the maximum power of 9297.8 w.

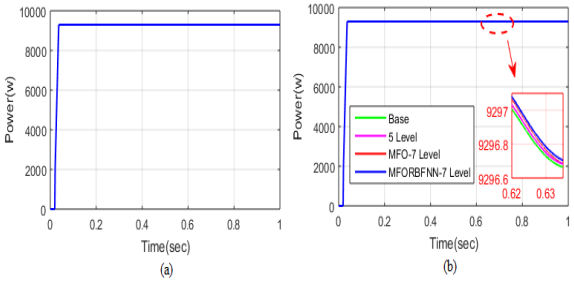

Fig. 16. (a) Load power of proposed controller (b) Load power comparison

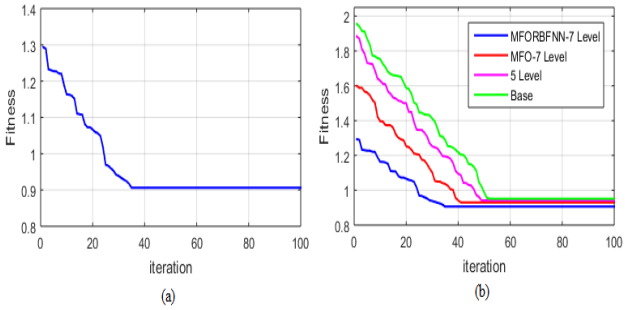

Fig. 17. Seven-level Inverter voltage of proposed controller

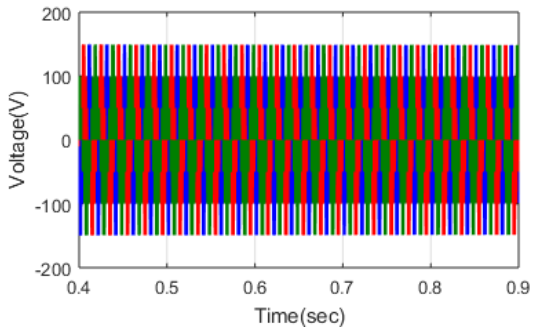

Fig. 18. Convergence Analysis (a) proposed controller (b) Comparison of Proposed controller and existing techniques

TABLE II
STATISTICAL ANALYSIS OF PROPOSED CONTROLLER WITH DIFFERENT TECHNIQUES FOR DEVIATION IN RENEWABLE ENERGY SOURCES

Solution Techniques	Mean	Median	S.D
Base	1.2145	0.9723	0.3253
5 Level	1.1538	0.9416	0.2858
MFO 7 Level	1.0643	0.9302	0.2065
MFO-RBFNN 7 Level	0.9681	0.9062	0.1099

Fig 17 plotted the seven-level inverter voltage of proposed controller. As seen from the fig 17, the seven-level inverter voltage achieves voltage range of 150 V at time instant of t=0.4 to 0.9 sec. Figure 18 (a) shows the fitness graph of proposed controller with iteration count of 100. As seen from the Fig 18 (a), in the count of iteration at 32, the fitness reaches the value of 0.9. The fitness comparison of proposed controller and the existing technique is plotted at figure 18 (b). It is observed from figure 18 (b), base method converge in the count of iteration at 50, 5 level inverter scheme converges in the count of iteration at 44, the MFO-7 level inverter scheme converges in the count of iteration at 40 and the proposed controller converges in the count of iteration at 32. Table 2 shows statistical analysis of proposed controller with different techniques for deviation in renewable energy sources. Table 2 tabulates the statistical analysis measures like mean, median, standard deviation. The proposed mean value is 0.9681, the median value of the proposed is 0.9062, and proposed standard deviation is 0.1099. On the overall analysis the proposed controller yields better power regulation than existing techniques. Moreover, proposed controller provides greater quality of solution.

VI. CONCLUSIONS

An innovative seven level inverter scheme for a grid connected HRES along proposed controller provided in this dissertation. The proposed MFO-RBFNN technique was developed to the control strategy purpose, which has the PI controller. At first, the currents are applied to the contribution of MFO algorithm and the error is minimized. From the output of MFO, the optimal gain parameter are created and shaped as a dataset. From that point forward, the optimal dataset is connected to the contribution of RBFNN, which is trained well and generated the control pulses. The proposed controller was executed at the work site of MATLAB/Simulink. The proposed controller performances are investigated with deviation in load condition and deviation in renewable energy sources. The results of comparison demonstrate the proposed controller is much better than other existing techniques to maximize the energy conversion of sources. Along this control method, the variation of system parameter as well as external disturbances was decreased; the load requirements were optimally met. The proposed controller provides a competitive performance based on the solution and computation time. Hence, proposed controller is a trustful technique to determine complexity issues as well as appearing to be strong and efficient method to maximize the energy sources.

REFERENCES

[1] S. Aissou, D. Rekioua, N. Mezzai, T. Rekioua and S. Bacha, "Modeling and control of hybrid photovoltaic wind power system with battery storage", *Energy Conversion and Management*, vol. 89, pp. 615-625, 2015.

[2] R. Gupta, R. Kumar and A. Bansal, "BBO-based small autonomous hybrid power system optimization incorporating wind speed and solar radiation forecasting", *Renewable and Sustainable Energy Reviews*, vol. 41, pp. 1366-1375, 2015.

[3] E. Romero-Cadaval, G. Spagnuolo, L. Franquelo, C. Ramos-Paja, T. Suntio and W. Xiao, "Grid-Connected Photovoltaic Generation Plants: Components and Operation", *IEEE Industrial Electronics Magazine*, vol. 7, no. 3, pp. 6-20, 2013.

[4] Q. Tabart, I. Vechiu, A. Etxeberria and S. Bacha, "Hybrid Energy Storage System Microgrids Integration for Power Quality Improvement Using Four-Leg Three-Level NPC Inverter and Second-Order Sliding Mode Control", *IEEE Transactions on Industrial Electronics*, vol. 65, no. 1, pp. 424-435, 2018.

[5] Y. Zheng, B. Jenkins, K. Kornbluth and C. Træholt, "Optimization under uncertainty of a biomass-integrated renewable energy microgrid with energy storage", *Renewable Energy*, vol. 123, pp. 204-217, 2018.

[6] M. Azharuddin Shamshuddin, T. Babu, T. Dragicevic, M. Miyatake and N. Rajasekar, "Priority-based Energy Management Technique for Integration of Solar PV, Battery, and Fuel Cell Systems in an Autonomous DC Microgrid", *Electric Power Components and Systems*, vol. 45, no. 17, pp. 1881-1891, 2017.

[7] A. Lorestani and M. Ardehali, "Optimal integration of renewable energy sources for autonomous tri-generation combined cooling, heating and power system based on evolutionary particle swarm optimization algorithm", *Energy*, vol. 145, pp. 839-855, 2018.

[8] Quan Li and P. Wolfs, "A Review of the Single Phase Photovoltaic Module Integrated Converter Topologies with Three Different DC Link Configurations", *IEEE Transactions on Power Electronics*, vol. 23, no. 3, pp. 1320-1333, 2008.

[9] C. Yeh and Y. Lai, "Digital Pulsewidth Modulation Technique for a Synchronous Buck DC/DC Converter to Reduce Switching Frequency", *IEEE Transactions on Industrial Electronics*, vol. 59, no. 1, pp. 550-561, 2012.

[10] R. Duan and J. Lee, "High-efficiency bidirectional DC-DC converter with coupled inductor", *IET Power Electronics*, vol. 5, no. 1, p. 115, 2012.

[11] G. Chandra Sekar, M. Rambabu, and A. Appa Rao, "Solar and Wind Energy Sources Interfacing to the Utillity Grid Using Five Level Inverter", International Journal of Engineering and Technology, Vol. 9, no. 2, pp. 502-509, 2017.

[12] G. Chandra Sekar, M. Rambabu, and A. Appa Rao, "Wind Energy Source Interfacing to Grid by Using Five-Level Inverter", International Journal of Control Theory and Applications, vol. 10, no. 5, pp. 577-587, 2017

[13] S. Jana and P. Biswas, "Numerical Computational analysis of supercapacitive storage with various type of loads to measure the response of five level inverter to integrate with lightning energy storage system", *2018 4th International Conference on Electrical Energy Systems (ICEES)*, 2018.

[14] B. Satish Naik, L. Umanand, K. Gopakumar and B. Subba Reddy, "A New Two-Phase Five-Level Converter for Three-Phase Isolated Grid-Tied Systems With Inherent Capacitor Balancing and Reduced Component Count", *IEEE Journal of Emerging and Selected Topics in Power Electronics*, vol. 6, no. 3, pp. 1325-1335, 2018.

[15] M. Shayestegan, M. Shakeri, H. Abunima, S. Reza, M. Akhtaruzzaman, B. Bais, S. Mat, K. Sopian and N. Amin, "An overview on prospects of new generation single-phase transformerless inverters for grid-connected photovoltaic (PV) systems", *Renewable and Sustainable Energy Reviews*, vol. 82, pp. 515-530, 2018.

[16] M. Sharifzadeh, H. Vahedi, R. Portillo, L. Garcia Franquelo and K. Al-Haddad, "Selective Harmonic Mitigation Based Self-Elimination of Triplen Harmonics for Single-Phase Five-Level Inverters", *IEEE Transactions on Power Electronics*, pp. 1-1, 2018.

[17] J. Kim, J. Kwon and B. Kwon, "High-Efficiency Two-Stage Three-Level Grid-Connected Photovoltaic Inverter", *IEEE Transactions on Industrial Electronics*, vol. 65, no. 3, pp. 2368-2377, 2018.

[18] A. Anurag, N. Deshmukh, A. Maguluri and S. Anand, "Integrated DC–DC Converter Based Grid-Connected Transformerless Photovoltaic Inverter With Extended Input Voltage Range", *IEEE Transactions on Power Electronics*, vol. 33, no. 10, pp. 8322-8330, 2018.

[19] M. di Benedetto, A. Lidozzi, L. Solero, F. Crescimbini and P. Grbovic, "Five-Level E-Type Inverter for Grid-Connected Applications", IEEE Transactions on Industry Applications, pp. 1-1, 2018.

[20] A. Sinha, K. Chandra Jana and M. Kumar Das, "An inclusive review on different multi-level inverter topologies, their modulation and control strategies for a grid connected photo-voltaic system", *Solar Energy*, vol. 170, pp. 633-657, 2018.

[21] G. Valderrama, G. Guzman, E. Pool-Mazun, P. Martinez-Rodriguez, M. Lopez-Sanchez and J. Zuniga, "A Single-Phase Asymmetrical T-Type Five-Level Transformerless PV Inverter", *IEEE Journal of Emerging and Selected Topics in Power Electronics*, vol. 6, no. 1, pp. 140-150, 2018.

[22] A. Ho and T. Chun, "Single-Phase Modified Quasi-Z-Source Cascaded Hybrid Five-Level Inverter", *IEEE Transactions on Industrial Electronics*, vol. 65, no. 6, pp. 5125-5134, 2018.

[23] A. Hota, S. Jain and V. Agarwal, "An Improved Three-Phase Five-Level Inverter Topology With Reduced Number of Switching Power Devices", *IEEE Transactions on Industrial Electronics*, vol. 65, no. 4, pp. 3296-3305, 2018

[24] X. Guo, J. Zhou, R. He, X. Jia and C. Rojas, "Leakage Current Attenuation of a Three-Phase Cascaded Inverter for Transformerless Grid-Connected PV Systems", *IEEE Transactions on Industrial Electronics*, vol. 65, no. 1, pp. 676-686, 2018.

[25] E. Grover-Silva, R. Girard and G. Kariniotakis, "Optimal sizing and placement of distribution grid connected battery systems through an SOCP optimal power flow algorithm", *Applied Energy*, vol. 219, pp. 385-393, 2018.

[26] A. Guichi, A. Talha, E. Berkouk and S. Mekhilef, "Energy management and performance evaluation of grid connected PV-battery hybrid system with inherent control scheme", *Sustainable Cities and Society*, vol. 41, pp. 490-504, 2018. https://doi.org/10.1016/j.scs.2018.05.026

[27] J. Chen, W. Zhang, J. Li, W. Zhang, Y. Liu, B. Zhao and Y. Zhang, "Optimal Sizing for Grid-Tied Microgrids With Consideration of Joint Optimization of Planning and Operation", *IEEE Transactions on Sustainable Energy*, vol. 9, no. 1, pp. 237-248, 2018.

[28] T. Ma, H. Yang, L. Lu and J. Peng, "Technical feasibility study on a standalone hybrid solar-wind system with pumped hydro storage for a remote island in Hong Kong", *Renewable Energy*, vol. 69, pp. 7-15, 2014.

[29] J. Rajaiah, V. Ramar and V. Parasunath, "Harmonic Minimization in Seven-Level Cascaded Multilevel Inverter Using Evolutionary Algorithm", *Circuits and Systems*, vol. 07, no. 09, pp. 2309-2322, 2016.

[30] Tae-Jin Kim, Dae-Wook Kang, Yo-Han Lee and Dong-Seok Hyun, "The analysis of conduction and switching losses in multi-level inverter system", *2001 IEEE 32nd Annual Power Electronics Specialists Conference (IEEE Cat. No.01CH37230).*

[31] S. Mirjalili, "Moth-flame optimization algorithm: A novel nature-inspired heuristic paradigm", *Knowledge-Based Systems*, vol. 89, pp. 228-249, 2015.

[32] B. Pham, A. Shirzadi, D. Tien Bui, I. Prakash and M. Dholakia, "A hybrid machine learning ensemble approach based on a Radial Basis Function neural network and Rotation Forest for landslide susceptibility modeling: A case study in the Himalayan area, India", *International Journal of Sediment Research*, vol. 33, no. 2, pp. 157-170, 2018.